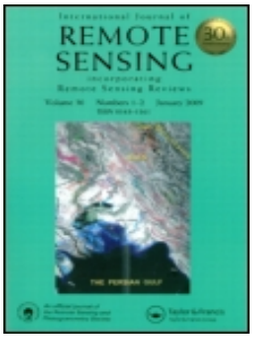

International Journal of Remote Sensing

ISSN: 0143-1161 (Print) 1366-5901 (Online) Journal homepage: http://www.tandfonline.com/loi/tres20

Measurement of water colour using AVIRIS imagery to assess the potential for an operational monitoring capability in the Pamlico Sound Estuary, USA

Ross S. Lunetta , Joseph F. Knight , Hans W. Paerl , John J. Streicher , Benjamin L. Peierls , Tom Gallo , John G. Lyon , Thomas H. Mace & Christopher P. Buzzelli

To cite this article: Ross S. Lunetta , Joseph F. Knight , Hans W. Paerl , John J. Streicher , Benjamin L. Peierls , Tom Gallo , John G. Lyon , Thomas H. Mace & Christopher P. Buzzelli (2009) Measurement of water colour using AVIRIS imagery to assess the potential for an operational monitoring capability in the Pamlico Sound Estuary, USA, International Journal of Remote Sensing, 30:13, 3291-3314, DOI: 10.1080/01431160802552801

To link to this article: http://dx.doi.org/10.1080/01431160802552801

Copyright Taylor and Francis Group, LLC

Published online: 22 Jul 2009.

Submit your article to this journal

Article views: 539

View related articles

Citing articles: 14 View citing articles

Full Terms & Conditions of access and use can be found at
http://www.tandfonline.com/action/journalInformation?journalCode=tres20

Download by: [University of North Texas] **Date:** 26 December 2016, At: 16:34

International Journal of Remote Sensing
Vol. 30, No. 13, 10 July 2009, 3291–3314

Measurement of water colour using AVIRIS imagery to assess the potential for an operational monitoring capability in the Pamlico Sound Estuary, USA

ROSS S. LUNETTA*†, JOSEPH F. KNIGHT**†, HANS W. PAERL‡, JOHN J. STREICHER§, BENJAMIN L. PEIERLS‡, TOM GALLO‡, JOHN G. LYON¶, THOMAS H. MACE†† and CHRISTOPHER P. BUZZELLI‡

†U.S. Environmental Protection Agency, National Exposure Research Laboratory, Research Triangle Park, NC 27711, USA

‡University of North Carolina at Chapel Hill, Institute of Marine Sciences, Morehead City, NC 28557, USA

§National Oceanic and Atmospheric Administration, On assignment to the U.S. Environmental Protection Agency, National Exposure Research Laboratory, Research Triangle Park, NC 27711, USA

¶U.S. Environmental Protection Agency, National Exposure Research Laboratory, 944 E. Harmon, Las Vegas, NV 89193, USA

††U.S. National Aeronautics and Space Administration, Office of the Associate Director for Operations, Dryden Flight Research Center, Edwards, CA 93523, USA

(*Received 14 November 2007; in final form 1 May 2008*)

The monitoring of water colour parameters can provide an important diagnostic tool for the assessment of aquatic ecosystem condition. Remote sensing has long been used to effectively monitor chlorophyll concentrations in open ocean systems; however, operational monitoring in coastal and estuarine areas has been limited because of the inherent complexities of coastal systems, and the coarse spectral and spatial resolutions of available satellite systems. Data were collected using the National Aeronautics and Space Administration (NASA) Advanced Visible–Infrared Imaging Spectrometer (AVIRIS) flown at an altitude of approximately 20 000 m to provide hyperspectral imagery and simulate both MEdium Resolution Imaging Spectrometer (MERIS) and Moderate Resolution Imaging Spectrometer (MODIS) data. AVIRIS data were atmospherically corrected using a radiative transfer modelling approach and analysed using band ratio and linear regression models. Regression analysis was performed with simultaneous field measurements data in the Neuse River Estuary (NRE) and Pamlico Sound on 15 May 2002. Chlorophyll *a* (Chl *a*) concentrations were optimally estimated using AVIRIS bands (9.5 nm) centred at 673.6 and 692.7 nm, resulting in a coefficient of determination (R^2) of 0.98. Concentrations of Chromophoric Dissolved Organic Matter (CDOM), Total Suspended Solids (TSS) and Fixed Suspended Solids (FSS) were also estimated, resulting in coefficients of determination of R^2=0.90, 0.59 and 0.64, respectively. Ratios of AVIRIS bands centred at or near those corresponding to the MERIS and MODIS sensors indicated that relatively good satellite-based estimates could

*Corresponding author. Email: lunetta.ross@epa.gov
** Current address: University of Minnesota, Department of Forest Resources, St Paul, MN 55108, USA.

International Journal of Remote Sensing
ISSN 0143-1161 print/ISSN 1366-5901 online © 2009 Taylor & Francis
http://www.tandf.co.uk/journals
DOI: 10.1080/01431160802552801

potentially be derived for water colour constituents at a spatial resolution of 300 and 500 m, respectively.

1. Introduction

Phytoplankton form the base of the food web within most open water aquatic systems. Their abundance and distribution represent important variables for understanding ecosystem processes and monitoring the condition of marine systems (Paerl *et al.* 2003). Phytoplankton can be partitioned into functional taxonomic groups (e.g. chlorophytes, cryptophytes, cynobacteria, diatoms and dinoflagellates) that play major roles in coastal production (Pinckney *et al.* 1998). Of particular interest is the occurrence of phytoplankton blooms, including dinoflagellate red tides, which can occur along highly populated coastal regions. Occurrences of dinoflagellate blooms have been positively correlated with high levels of Chromophoric (coloured) Dissolved Organic Matter (CDOM) (Gilbert and Terlizzi 1999). Dinoflagellates are also able to undergo photosynthetic photoadaption response (increased pigmentation), and are therefore able to maintain photosynthetic capacity at lower light levels (Prezelin and Alberte 1978).

Water colour associated with estuarine systems is typically characterized by high levels of Total Suspended Solids (TSS), CDOM and chlorophyll, exhibiting a complex mixture of contributing colour constituents (Bukata *et al.* 1995). Waters are designated as Case 2 when colour constituents other than chlorophyll are optically significant and vary independently. Conversely, open ocean environments are commonly characterized by relatively low levels of TSS, CDOM and chlorophyll, with chlorophyll being the principal colourant. Algorithms developed to estimate chlorophyll in open ocean systems have not typically accounted for the presence of high concentrations of CDOM and TSS, which persist in many estuarine systems. To overcome the spectral interference caused by TSS and CDOM, numerous researchers have demonstrated the utility of the chlorophyll *a* (Chl *a*) absorption maximum near 673 nm to enhance retrieval performance in optically complex systems (Neville and Gower 1977, Thiemann and Kaufmann 2000, Shafique *et al.* 2003).

Satellite remote sensor systems and approaches for chlorophyll retrials have included the development of reflectance (R) ratios for the Coastal Zone Colour Scanner (CZCS) (R_{520}/R_{550}) and the Sea-viewing Wide Field-of-view Sensor (SeaWiFS) (OC4 $R_{\max}$ (R_{445}/R_{555}, R_{490}/R_{555}, R_{510}/R_{555} and R_{670}/R_{550}) sensors; O'Reilly *et al.* 2000). However, in coastal areas high TSS concentrations can cause interference (maximum reflectance near 550 nm). Herut *et al.* (1999) attempted to alleviate the TSS problem by calculating an R_{baseline} across the spectral ranges adjacent to the Chl *a* absorption and fluorescence features (667–748 nm). Hoogenboom *et al.* (1998) determined that a ratio using an Advanced Visible–Infrared Imaging Spectrometer (AVIRIS) band located near 713 nm with the band at 667 nm was the most sensitive for Chl *a* retrieval for inland waters. A similar ratio (R_{674}/R_{705}) has been demonstrated to be optimal for inland lakes and rivers (Thiemann and Kaufmann 2000, Shafique *et al.* 2003) and the MEdium Resolution Imaging Spectrometer (MERIS) standard Chl *a* retrieval algorithm uses R_{665}/R_{708} (Gons *et al.* 2005). Alternatively, the development of inverse bio-optical models to derive the concentrations of all three water colour constituents (i.e. suspended matter, total chlorophyll and CDOM) simultaneously could provide for improvements over a single parameter approach (Schiller and Doerffer 1999, Karaska *et al.* 2004).

The SeaWiFS OC4 chlorophyll retrieval algorithm has been found to generally overestimate chlorophyll concentrations for waters with high CDOM concentrations

(Liew *et al.* 2001). Field reflectance data collected from turbid inland lakes used to simulate ratios incorporating both the SeaWiFS and Moderate Resolution Imaging Spectrometer (MODIS) near-infrared (NIR) bands indicated that the NIR can potentially provide improved quantitative estimates of chlorophyll concentrations, provided that an atmospheric correction in the NIR spectral region is first performed. The results indicated that the SeaWiFS band ratio R_{670}/R_{765} (R^2=0.86, n=61) and MODIS R_{667}/R_{748} (R^2=0.90, n=61) gave the best results (Dall'Olmo *et al.* 2005). The standard Chl *a* algorithm developed for MERIS exploits the reflectance ratio R_{665}/R_{708} (Chl *a* absorption) and incorporates a correction for water absorption using band 12 (776 nm) to derive the total backscattering coefficient (Gons *et al.* 2005). For hyperspectral data, the process of selecting a band ratio for application can best be performed by selecting the primary band at the absorption or reflectance feature maxima and the second longer wavelength to provide a baseline with minimal variability (Ruddick *et al.* 2001).

CDOM, also known as yellow substance or gelbstoff, is an important water colour parameter for the study of near-coastal and estuarine biological processes. CDOM can be used along with Chl *a* to further refine harmful algal bloom (HAB) predictions, indicate the input and distribution of terrestrial organic matter, and contribute to the broad-scale understanding of biogeochemical processes. CDOM absorbs light at both ultraviolet (UV) and visible wavelengths, which means it controls light available for primary production, protects against UV damage to biota, and is subject to photooxidative degradation, resulting in greenhouse gas production and the release of biologically available organic matter and nutrients. Measurement data from Black Sea cruises between September 1993 and 2001 indicated that the log-transformed ratio R_{490}/R_{590} resulted in a CDOM coefficient of determination of R^2=0.63, n=577 (Kowalczuk *et al.* 2004). Satellite remote sensing of inland lake CDOM resulted in a coefficient of determination R^2 ranging from 0.73 to 0.83 in two separate experiments using Advanced Land Imager (ALI) data and a ratio incorporating bands 2 and 3 ($R_{525–605}/R_{630–690}$) (Kutser *et al.* 2005). Hu *et al.* (2004) reported a reasonably good correlation between CDOM and MODIS moderate-resolution (500 m) data bands R_{469}/R_{555} (R^2=0.8, n=31) for the Tampa Bay Estuary, Florida.

TSS concentrations regulate light attenuation, and suspended sediment impacts submerged aquatic vegetation (SAV) habitats, particularly in estuarine systems. Satellite remote sensing has also been used to estimate the concentrations of surface TSS. Lyon *et al.* (1988) determined that Landsat and Advanced Very High Resolution Radiometer (AVHRR) imagery could be used to categorize surface sediment concentration trends that corresponded with hydrodynamic and water quality model simulations for Sandusky Bay, Lake Erie. More recently, Miller and McKee (2004) demonstrated the application of MODIS (Terra) 250 m data to quantify TSS using a linear regression model relationship established between MODIS band-1 (620–670 nm) and *in situ* measurements of concentrations of inorganic-dominated TSS or Fixed Suspended Solids (FSS) in the coastal northern Gulf of Mexico (R^2=0.89, n=52).

2. Study area

The Albemarle-Pamlico Estuarine System (APES) is the second largest estuary in the USA, measuring approximately 52 000 km^2. The system is composed of four major riverine sub-estuaries and contains five major ecoregions (Omernik 1987). The

sub-estuaries, as well as the receiving Pamlico Sound, are nutrient sensitive, and because of the lagoonal nature of the system, it exhibits long water residence times. This, combined with periodic strong vertical stratification, makes the system susceptible to negative impacts of nutrient overenrichment, including algal blooms and bottom water hypoxia (Paerl *et al.* 1998, 2001). Priority environmental issues include neurotoxic shellfish poisoning (due to *K. brevis*), fish kills, and seagrass die-off. The Neuse River Estuary (NRE) is the largest of the four APES tributaries. The Neuse River and neighbouring Pamlico Sound Estuaries are subject to significant nutrient and sediment loading from the Neuse and Tar River Basins. The offshore flow of sediments is restricted by the barrier islands of the Outer Banks.

3. Study objectives

This study sought to determine the potential applications of airborne AVIRIS and MERIS and MODIS satellite remote sensor data to support the operational monitoring of water colour constituents in the APES. Specifically, our objective was to use AVIRIS hyperspectral airborne imagery to explore optimal band(s) for water quality estimates and to simulate MERIS and MODIS satellite data for operational monitoring of major water colour constituents (i.e. Chl *a*, CDOM and TSS). We evaluated the performance of existing methods calibrated specifically for the APES (using *in situ* measurement data, airborne and simulated satellite remote sensor data) to determine the potential for establishing an operational water quality monitoring capability for monitoring both natural processes and the outcomes of regulatory actions on estuarine indicators of water quality.

Targeted operational applications include monitoring the impact of the Neuse River Basin Total Maximum Daily Load (TMDL) nitrogen source reduction allocations developed to reduce maximum Chl *a* concentration below 40.0 $\mu g\,l^{-1}$. An additional objective was to determine the potential for monitoring Chl *a* and CDOM concentrations to provide a means for identifying probable locations for HAB development. Finally, we investigated the potential for remote sensor TSS measurements to support SAV impact assessments related to potential sedimentation exposure. To accomplish these objectives we used high-altitude airborne hyperspectral data to evaluate the potential of both airborne and satellite (MERIS and MODIS) data to support the operational measurement capability for the major water colour constituents across the Neuse River and Pamlico Estuaries in NC.

4. Methods

The approach used in this study included the simultaneous acquisition of high-altitude airborne hyperspectral imagery, atmospheric optical measurements, and *in situ* water samples. Hyperspectral imagery was atmospherically corrected to surface reflectance using a radiative transfer modelling approach detailed below. Water quality measurements were made using standard fluorometric techniques and phytoplankton pigments were analysed using high-performance liquid chromatography (HPLC) to identify and quantify photosynthetic pigments at 13 sampling sites in the NRE and Pamlico Sound. The remote sensor data were analysed with the water quality and HPLC-derived pigment concentration data to determine the coefficient of determination for estimating water colour constituent concentrations using the airborne hyperspectral data. MERIS and MODIS satellite data were simulated by selecting the AVIRIS band(s) that most closely corresponded to

specific MERIS and MODIS application bands. The MERIS- and MODIS-simulated data were first analysed at a nominal spatial resolution of 17 m × 17 m to facilitate regression analysis with available *in situ* water quality measurement data. Analytical methods applied included both band ratios and single-band linear regression models. Finally, the simulated MERIS results were aggregated (simple average) to 300 m × 300 m to assess the potential utility of satellite-scale observation data for characterizing estuarine condition and processes for operational applications in the APES (table 1).

4.1 *Imagery collection*

AVIRIS hyperspectral imagery was acquired from the National Aeronautics and Space Administration (NASA) Earth Resources 2 (ER-2) aircraft for the Neuse River and Pamlico Sound Estuaries on 15 May 2002, between 14:09 and 15:54 GMT. The AVIRIS sensor, which has 224 contiguous spectral bands within the 400–2500 nm range, has a signal-to-noise (SNR) of approximately 1000 : 1 in the visible and near-infrared (VNIR) spectrometer and variable band widths ranging from 9.4 to 12.5 nm. The flight altitude of the ER-2 aircraft was 20 000 m, providing a nominal pixel resolution of approximately 17 m × 17 m. The NRE flight line was flown at 158° heading with a solar zenith angle (SZA) of 28°. All Albemarle-Pamlico flight lines were flown at a 110° heading with an SZA ranging from 23° to 41°.

The day prior to data collections (14 May 2002) a frontal system passed through the study area from the northwest providing relatively clear atmospheric conditions on the date of the overflight. On the morning of 15 May 2002, winds were out of the northwest at 8.0 kts (4.0 m s^{-1}) under cloudless sky conditions.

4.2 *Field data*

Two boats were used to collect water samples at the 13 sampling sites during the time of the ER-2 overpass (figure 1). One boat sampled from site NR30 to PS1 and the second from site PS3 to NOAA5. Three surface water samples were collected at each site and the measured values were averaged to derive reported values. Chl *a* concentrations were measured using *in vitro* fluorescence following the non-acidification modification of the EPA method 445.0 (Arar and Collins 1997). This method uses narrow bandpass excitation and emission filters to eliminate interference from Chl *b* and pheopigments (Welschmeyer 1994). Phytoplankton photopigment concentration and community composition were determined using chromatography and diagnostic photopigment analyses (Millie *et al.* 1993, Tester *et al.* 1995, Jeffrey *et al.* 1997, Paerl *et al.* 2003). Sample aliquots (0.5 l) collected from the 13 field stations were filtered using 47 mm Whatman GF/F filters, and frozen (−80°C). The filters were placed in 100% acetone, sonicated, and extracted for 18–24 h. HPLC was used to quantify selected biomarker algal pigments (chlorophylls and carotenoids) (Millie *et al.* 1993, Jeffrey *et al.* 1997, Li *et al.* 2002). An in-line photodiode array spectrophotometer (Shimadzu SPD M10avp) provided photopigment identification based on retention time and characteristic absorption spectra from 380 to 700 nm, and concentration based on chromatograms at 440 nm (Rowan 1989).

The matrix factorization program CHEMical TAXonomy (CHEMTAX) was used to quantify the relative biomass, expressed as percentage of total Chl *a*, for major algal groups (cyanobacteria, diatoms, chlorophytes, cryptophytes and

Table 1. The channel numbers, band centre wavelengths, band widths, resolution and signal-to-noise ratios (SNR) for the AVIRIS (Kruse 2003), MERIS (Drinkwater and Rebhan 2005) and MODIS (Carder *et al*. 2003) instruments. Although MERIS data are available in both full (300 m) and low (1200 m) resolutions, only full-resolution data were used in this study. The repeat frequency for MERIS collections is 2–3 days and for MODIS 1–2 days.

Channel	Wavelength (nm)	Band width (nm)	Resolution (m)	SNR
AVIRIS (subset of 224 channels)				
8	442.1	10.5	20	~1000 : 1
11	470.9	10.3	20	~1000 : 1
13	490.2	10.1	20	~1000 : 1
15	509.5	10.0	20	~1000 : 1
20	558	9.7	20	~1000 : 1
26	616.2	9.6	20	~1000 : 1
27	626	9.6	20	~1000 : 1
28	635.7	9.6	20	~1000 : 1
29	645.4	9.6	20	~1000 : 1
30	655.1	9.7	20	~1000 : 1
31	664.8	9.7	20	~1000 : 1
35	673.6	9.5	20	~1000 : 1
36	683.2	9.5	20	~500 : 1
37	692.7	9.5	20	~500 : 1
39	711.7	9.5	20	~500 : 1
40	721.3	9.5	20	~500 : 1
41	730.8	9.5	20	~500 : 1
42	740.4	9.5	20	~500 : 1
43	750	9.6	20	~500 : 1
44	759.5	9.6	20	~500 : 1
45	769.1	9.6	20	~500 : 1
46	778.7	9.7	20	~500 : 1
47	788.3	9.8	20	~500 : 1
48	797.9	9.8	20	~500 : 1
49	807.5	9.9	20	~500 : 1
50	817.1	10.0	20	~500 : 1
51	826.7	10.1	20	~500 : 1
52	836.3	10.2	20	~500 : 1
53	845.9	10.3	20	~500 : 1
54	855.5	10.4	20	~500 : 1
55	865.1	10.5	20	~500 : 1
56	874.7	10.7	20	~500 : 1
73	1041	9.3	20	~500 : 1
94	1239.5	9.5	20	~500 : 1
MERIS (all channels)				
1	412.5	10	300	468 : 1
2	442.5	10	300	413 : 1
3	490	10	300	355 : 1
4	510	10	300	306 : 1
5	560	10	300	289 : 1
6	620	10	300	216 : 1
7	665	10	300	177 : 1
8	681.3	7.5	300	147 : 1
9	709	9	300	158 : 1
10	753.8	7.5	300	101 : 1
11	760.6	3.75	300	375 : 1
12	775	14	300	157 : 1
13	865	20	300	114 : 1
14	885	10	300	113 : 1
15	900	10	300	51 : 1

Table 1. (*Continued.*)

Channel	Wavelength (nm)	Band width (nm)	Resolution (m)	SNR
MODIS (first 19 channels)				
1	645	50	250	128 : 1
2	858.5	35	250	201 : 1
3	469	20	500	243 : 1
4	555	20	500	228 : 1
5	1240	20	500	74 : 1
6	1640	24	500	275 : 1
7	2130	50	500	110 : 1
8	412	15	1000	880 : 1
9	443	10	1000	838 : 1
10	488	10	1000	802 : 1
11	531	10	1000	754 : 1
12	551	10	1000	750 : 1
13	667	10	1000	910 : 1
14	678	10	1000	1087 : 1
15	748	10	1000	586 : 1
16	869.5	15	1000	516 : 1
17	905	30	1000	167 : 1
18	936	10	1000	57 : 1
19	940	50	1000	250 : 1

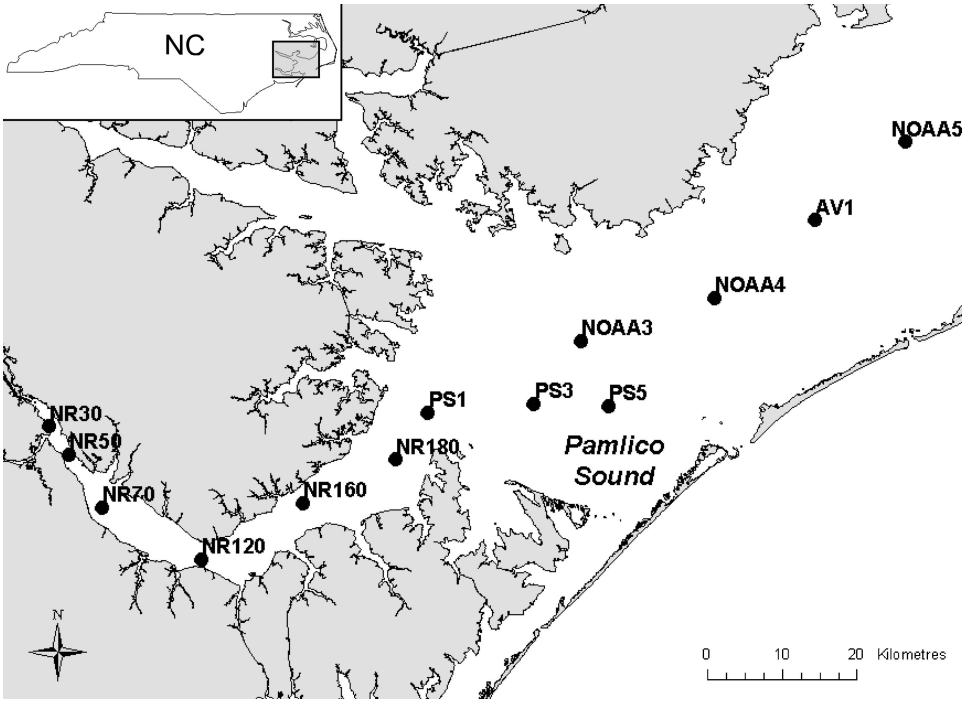

Figure 1. Study site including the Neuse River Estuary and Pamlico Sound field water sample locations.

dinoflagellates) represented in the phytoplankton community (Mackey *et al.* 1996, 1997, Wright *et al.* 1996, Pinckney *et al.* 2001). The input for the program was the photopigment concentrations obtained from HPLC and an experimentally derived initial photopigment ratio file. The program used a steepest decent algorithm to determine the best fit of the observed photopigment concentrations to the ratios in the major algal classes as defined in the initial photopigment ratio file.

CDOM was measured on filtered (Whatman GF/F) aliquots from each sample using a Turner TD-700 fluorometer configured with a near-UV mercury vapour lamp, a 350 nm excitation filter, and a 410–600 nm emission filter. The fluorometer was calibrated to quinine sulfate (QS) solutions made up in 2 N sulfuric acid. CDOM concentrations were reported as μg QS per litre. TSS was measured gravimetrically using the protocol outlined by the Water Environment Federation (WEF 1998). Precombusted (450°C, 4 h) and preweighed Whatman GF/F filters were used to filter 0.5 l of each sample. Filter weights were determined after overnight drying at 95°C. TSS concentrations (mg l^{-1}) were calculated from the volumetric weight difference and FSS was the weight difference after furnace ignition at 550°C.

5. Atmospheric corrections

The objective of atmospheric correction of the AVIRIS imagery was to derive surface reflectance from measured upwelling radiance at sensor. The proportionality describing radiance at a nadir-viewing sensor was as:

$$L_{\mathrm{Sensor}}(\lambda) \propto L_{\mathrm{Sun}}(\lambda) T(\lambda) R(\lambda) + L_{\mathrm{Path}}(\lambda) \tag{1}$$

where λ is the wavelength, $L_{\mathrm{Sensor}}(\lambda)$ is the radiance at the sensor, $L_{\mathrm{Sun}}(\lambda)$ is the solar radiance above the atmosphere, $T(\lambda)$ is the total path atmospheric transmittance, $R(\lambda)$ is the surface reflectance, and $L_{\mathrm{Path}}(\lambda)$ is the path scattered (i.e. backscattered) radiance. The radiance signal at the sensor was composed of solar backscattered radiation from the atmosphere and an attenuated signal component originating from the surface. Therefore, atmospheric correction was necessary to remove the backscattered 'noise' and enhance the surface signal.

The correction method used a look-up table (LUT) approach, using the MODTRAN (Berk *et al.* 1989) radiative transfer model to generate tables of upwelling radiance (as a function of wavelength) corresponding to the range of surface reflectances, atmospheric aerosol loadings and water vapour that would anticipate the range of observed radiances in the study region. All radiative transfer calculations used the discrete ordinate method and included multiple scattering (Stamnes and Conklin 1984).

The base atmospheric model used for all simulations was the U.S. Air Force Geophysical Laboratory Midlatitude Summer atmosphere (AFGLMS). MODTRAN radiance calculations were performed for altitudes of 20 km above sea level (asl), the nominal altitude of the AVIRIS imaging. The composition of atmospheric gases was retained unaltered from their values in the AFGLMS model. Modelled tropospheric aerosol loading ranged from a surface visibility of 5–23 km, with aerosol type being a mixture of 70% rural and 30% oceanic. (The prior 24-h wind direction was northwesterly, indicating a predominantly rural aerosol type from the continental land mass.) Modelled precipitable water vapour ranged from 1.46 to 4.38 cm, corresponding to 0.5 and 1.5, respectively, times the base model atmosphere's precipitable water vapour. The modelled surface reflectance ranged from 0.00 to 1.00. Because of the extremely low reflectance

of water (relative to land), and the importance of even small variations in water reflectance to the study objectives, the modelled surface reflectances were incremented logarithmically rather than linearly, to better resolve small differences at low reflectances. Thus, upwelling radiances were modelled for surfaces with nominal reflectances of 0.00, 0.01, 0.02, 0.05, 0.10, 0.20, 0.50 and 1.00. In total, 32 LUTs ($2 \times 2 \times 8$) were created to span the range of observed radiance measurements.

An initial classification of each pixel as land or water was necessary prior to atmospheric correction so that appropriate algorithms for sun glint, water vapour and aerosol correction could be applied. This determination was made using threshold criteria that were applied to the radiance values at four atmospheric window bands (765, 865, 1040 and 1240 nm). Establishing appropriate radiance thresholds for water *versus* land was accomplished using trial and error subject to visual inspection of the imagery (Land and Haigh 1996). The threshold criteria that were applied corresponded to 5.0% surface reflectance at 20 km asl for a 0.4 aerosol optical depth (AOD) at 550 nm. The independent testing of radiance thresholds at four bands, while redundant, provided a greater level of confidence in the classification. Following pixel land/water classification, algorithms for the determination of aerosol (as visibility) and water vapour content were executed. Knowing the aerosol and water vapour content of a pixel enabled a refined determination of surface reflectance. A final set of eight hybrid radiance LUTs (one for each nominal reflectance value, listed above) were created for the pixel undergoing atmospheric correction, matching the aerosol loading and precipitable water vapour content of that pixel.

The 'inverse problem' (retrieval of surface reflectance from at-sensor radiance) was then solved by comparing the observed AVIRIS pixel radiance at each band to the modelled radiances that bounded it at lower and higher radiance (Green 1991). Linear interpolation between the bounding radiances was used to determine the surface reflectance of the observed pixel. The small increments in modelled reflectance served to minimize errors associated with using a piecewise linear interpolation approach to reflectance determination in the highly nonlinear radiance/reflectance functional relationship. The spatial precision of the correction was pixel-wise (17 m × 17 m) for water vapour, and 100 m × 100 m for aerosol correction.

5.1 *Sun glint*

The SZA during the AVIRIS data collection ranged from 41° to 23°. Based solely on solar zenith and azimuth angles, sun glint was not expected. However, wind speed during the day was reported at Beaufort and Cape Hatteras at 8.0 kts from the northwest. The APES was slightly turbulent, with wave action distorting the surface sufficiently to cause a moderate degree of sun glint to appear in five of the six flight lines. From a signal processing perspective, glint is a radiance noise term superimposed over a radiance signal (Cox and Munk 1954, Gordon and Wang 1994).

The specular reflection had contributions from both direct (sun beam) and Rayleigh-scattered skylight. The unique signature of specularly reflected direct sunlight appears as a non-isotropic increase in radiance from nadir to the direction of the solar aziumuth. Specularly reflected Rayleigh-scattered skylight has no unique signature that would distinguish it from diffusely reflected surface irradiance; hence it was not possible to remove its contribution. The contribution

of specularly reflected direct sunlight (i.e. glint) to the radiance signal was removed prior to atmospheric correction. Baseline (non-glinted) radiance was determined by averaging the mean spectral radiance over the glint-free part of the scene observed looking away from the sun. Pixels corresponding to off-nadir views that were greater than 90° of the solar azimuth angle were assumed to be relatively undegraded.

The minimum SZA during the AVIRIS data collect was approximately 23° (with solar azimuth at 131°) and maximum approximately 41° (with solar azimuth at 103°). Thus the sun, and hence the forward scattered glint, was always between the east and the southeast. The critical aspect was to fit a regression function to an observed trend of increasing spectral radiance for any row of pixels, beginning from a nadir-view pixel, to off-nadir pixels in the same row in the direction of increasing glint. Baseline radiance was determined at all bands for each row of the image that viewed water. The baseline was calculated as the mean spectral radiance for those water pixels unaffected by glint. A unique regression equation was created for each row, and for each band, to numerically characterize the increase in spectral radiance across the scene (i.e. the glint component of radiance), relative to the baseline. The band-specific and row-specific regression function was then used to subtract the glint component from the radiance at each pixel. To characterize the noise component of the total radiance, a regression function for each band was fit to each line of the image. The form of the regression function equated total radiance to an exponential function of linear distance across the scene. The true reflectance, and therefore upwelling radiance, of the water was assumed to have no net trend across the flight line.

5.2 *Water vapour and aerosol corrections*

Atmospheric precipitable water content was determined using a band ratio method (Bruegge *et al.* 1990, Green 1999). The upwelling radiance at 902 nm (a band strongly attenuated by water vapour) was divided by the upwelling radiance at 865 nm (a band for which water vapour is transparent). Thus, the resulting quotient was compared to reference atmospheres of known water content (i.e. LUTs), and the precipitable water vapour in the vertical column above a given pixel was determined (Gao and Goetz 1990).

The determination of AOD over Case 1 or Case 2 waters required unique algorithms (Dekker *et al.* 1997). For Case 1 waters the determination of AOD is greatly simplified by taking advantage of the known zero reflectance for NIR bands; hence all upwelling radiance in those bands may be attributed to atmospheric backscatter. However, for Case 2 waters, there are no wavelengths that consistently have zero reflectance due to the presence of variable concentrations of suspended solids. The algorithm developed here to determine aerosol loading over the APES waters used four IR bands to make an assessment of AOD.

The algorithm incorporated bands at 769.1, 865.1, 1041 and 1239.1 nm, which corresponded to atmospheric windows with respect to gases and water vapour (Green *et al.* 1993, Vermote *et al.* 2002). While the NIR 769.1 nm band would have been most sensitive to aerosol scattering, the reflectance was least likely to be zero. Conversely, the 1239.5 nm band was expected to have near-zero surface reflectance, but with the scattering effects of aerosols being small. A pixel-wise AOD was calculated for each selected band and the final assignment assumed that strong mixing in the lower atmosphere would not support significant aerosol concentration gradients. Therefore, any variation in calculated AOD within a small cluster of pixels

was due to a non-zero surface reflectance. Thus, the smallest computed AOD corresponding to any of the above IR bands within a cluster (5×5 pixels) was deemed to be the best estimate (the suspended solids could only bias the calculation towards higher AOD). The mean AOD over the entire study area was determined to be approximately 0.4 in the visible spectrum.

6. Chl *a*

Estimated Chl *a* concentrations for the 13 field sites were determined by computing band ratios using the AVIRIS data. Spectral band ratios were applied to capture the depth of the Chl *a* absorption maximum occurring at 673.6 nm. To determine the best band combinations for estimating Chl *a* concentrations, a number of band ratios incorporating both the absorption maximum and red-edge baseline were correlated with the measured water sample concentrations for the 13 field sample sites. The correlations were established using the Pearson determination coefficient (R^2). Finally, the AVIRIS Chl *a* ratio was used as the independent variable and the measured Chl *a* concentration from the 13 field sample sites as the dependent variable in a linear regression model to generate concentration estimates corresponding to individual AVIRIS pixels across the study area. The optimal Chl *a* regression equation obtained was:

$$f_{\text{Chl-}a} = 60.24(R_{693}/R_{673}) - 58.58 \tag{2}$$

where $f_{\text{Chl-}a}$ is the estimated concentration of Chl *a* for a given pixel of the AVIRIS image.

Data corresponding to the MERIS bands (B) were simulated for Chl *a* estimates using the AVIRIS channels (31, 36 and 39) centred at 664.8 nm (B7), 683.2 nm (B8) and 711.7 nm (B9). Linear regression analysis was performed using $R_{664.8}/R_{711.7}$ corresponding to the Chl *a* secondary absorption feature and $R_{683.2}/R_{711.7}$ corresponding to the Chl *a* fluorescence feature. The AVIRIS band centred at 665.1 nm corresponded very well with the MERIS band location and width (9.7 nm). However, the AVIRIS channel located at 683.2 nm was centred at a slightly longer wavelength compared to that of MERIS (681.3 nm), but had a similar bandwidth (10 *vs.* 9.7 nm, respectively).

Similarly, data corresponding to the MODIS bands (B) were simulated for Chl *a* estimates using the AVIRIS channels (11 and 20) centred at 470.9 nm (B3) and 558 nm (B4). Simple linear regression analysis was performed using $R_{470.9}/R_{558}$ (Hu *et al.* 2004). The AVIRIS channels was centred at a slightly longer wavelengths compared to that of MODIS B3 (469 nm) and B4 (555 nm) had a significantly narrower bandwidth compared to MODIS (approximately 10 *vs.* 20 nm).

6.1 *SeaWiFS algorithms*

The results of the Chl *a* concentration estimation approach outlined above were compared with estimates generated by the SeaWiFS OC4 and Case 2 waters Chl *a* algorithms. The OC4 algorithm is as follows (O'Reilly *et al.* 1998):

$$\log 10(\text{Chl-}a_4) = a_0 + a_1 L + a_2 L^2 + a_3 L^3 \tag{3}$$

where $L = \log_{10}(R_{\max})$, $R_{\max} = \max(R_{443}/R_{555},\ R_{490}/R_{555},\ R_{510}/R_{555})$, $a_0 = 0.4708$, $a_1 = -3.8469$, $a_2 = 4.5338$, $a_3 = -2.4434$ and $a_4 = -0.0414$. The SeaWiFS Case 2 algorithm uses the band ratio R_{670}/R_{555} (Xiaoxiang *et al.* 2004). The ratio is

augmented with coefficients derived from location specific regression analysis using calibration data. The development of site specific coefficients for the measurement of Chl *a* in Case 2 waters is required because of the wide variability in water colour constituents encountered in coastal ocean environments.

7. CDOM and TSS

CDOM values were estimated using the band ratios reported by Kutser *et al.* (2005) developed for lake systems in Finland and Sweden and by Hu *et al.* (2004) developed for the Tampa Bay Estuary in Florida. The Kutser *et al.* (2005) algorithm was originally developed for application using the Advanced Land Imager (ALI); the ratio incorporated ALI band-2 (525–605 nm) and band-3 (630–690 nm). We adapted the ratio by averaging the AVIRIS bands that most closely corresponded to ALI band-2 (eight-band average) and band-3 (six-band average). To simulate the Hu *et al.* (2004) MODIS algorithm we used AVIRIS channels (11 and 20) centred at 470.9 nm to represent MODIS band-3 (469 nm) and band-4 (558 nm).

Both TSS and FSS were estimated by applying the method reported by Miller and McKee (2004) that was developed for Lake Pontchartrain, the Mississippi Delta and Sound areas. They determined that a linear regression approach using MODIS band-1 (620–670 nm) provided a robust monitoring capability for a clay-silt (inorganic) dominated system. This approach was applied by averaging four AVIRIS bands to simulate the MODIS 620–670 nm bandpass. To best simulate the CDOM ALI ratio corresponding to MERIS, the AVIRIS bands centred at 558 and 665.1 nm (R_{557}/R_{665}) were used. This corresponded very closely to the MERIS bands 5 and 7 (B5/B7). TSS linear regression analysis was performed using the AVIRIS band centred at 616 nm to simulate the MERIS band-6 (620 nm).

8. Results

The results of the atmospheric corrections are illustrated by the three AVIRIS surface reflectance graphs that represent the range of water colour conditions across the 13 water quality sampling stations on 15 May 2002 (figures 2(*a*)–2(*c*)). The modelled surface reflectance was a function of surface water colour constituents integrated across each 17 m AVIRIS pixel. Subsequent to the application of the radiative transfer model, the general surface reflectance features including reflectance peaks and absorption features can be discerned. Also evident is the loss of signal (zero reflectance) in the lower blue (<423 nm) part of the spectrum as a result of high CDOM absorption. Figure 2(*a*) illustrates the high reflectance in the blue (442 nm) and green (565 nm) wavelengths as a result of low Chl *a* and CDOM, and relatively high TSS concentrations for NOAA3. Figures 2(*b*) and 2(*c*) illustrate the absorption impacts of CDOM associated with increasing concentrations (30.0>51.8 μg QS l^{-1}). These interferences are particularly significant over water due to the inherently low levels of reflectance (figures 2(*a*)–2(*c*)).

8.1 *Chl a*

Table 2 lists the main water quality parameters measured for the 13 field sites, including start and end sampling times for Chl *a*, CDOM and TSS. These data indicated that the highest Chl *a* and CDOM concentrations occurred in the upper NRE sites (NR30, NR50 and NR70). Total Chl *a* values ranged from 29.3 to 42.9 μgl^{-1} and CDOM from 40.6 to 60.3 μg QS l^{-1}. Table 3 shows the fraction of

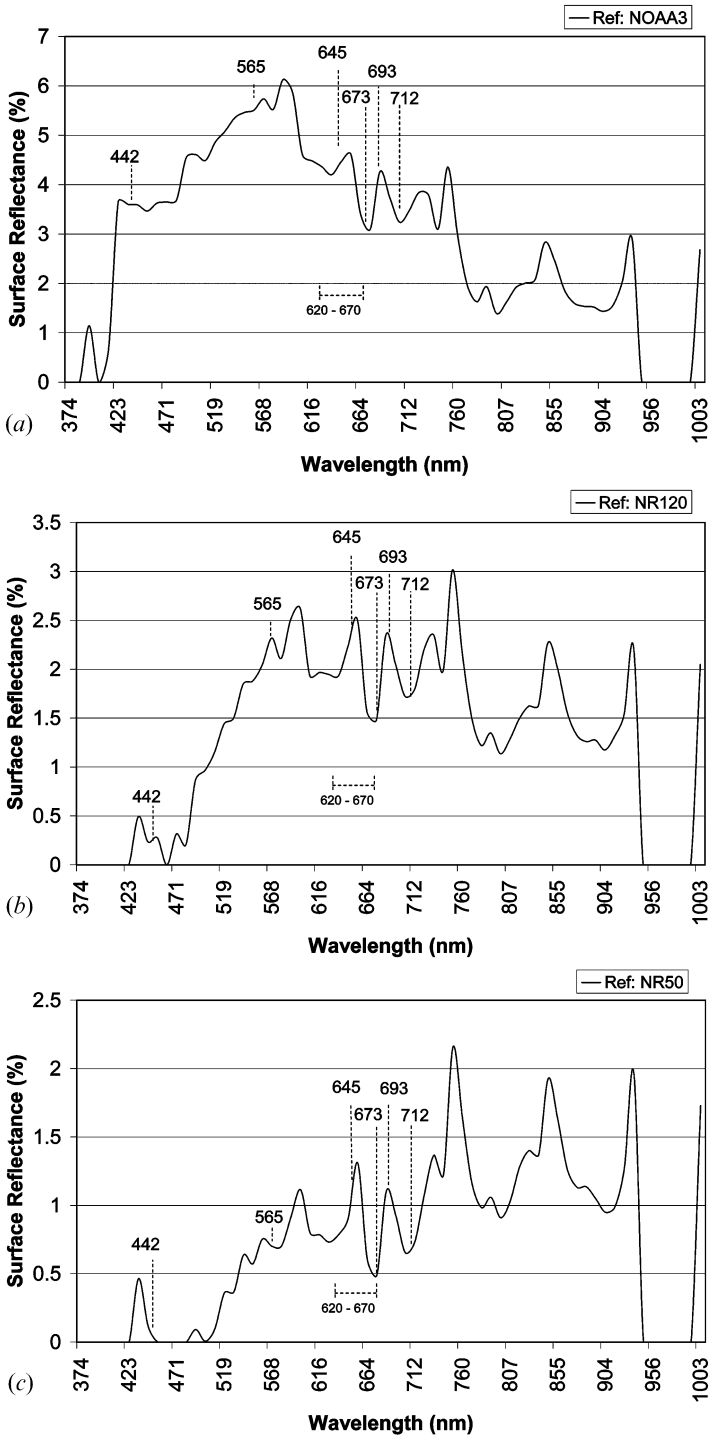

Figure 2. AVIRIS atmospherically corrected surface reflectance data for sites (*a*) NOAA3, (*b*) NR120 and (*c*) NR50. These reflectance graphs represent the range of conditions that existed across the 13 sampling sites on 15 May 2002.

Table 2. Neuse River Estuary and Pamlico Sound water quality sample data for 15 May 2002. Salinity gradients are reported as the percentage difference between surface and bottom measurements. Sampling sites are reported in eastern daylight time (EDT) beginning in the upper Neuse River, then extending down river and into the Neuse River and Pamlico Estuary. The diffuse attenuation coefficient (K_d) was based on photosynthetically active radiation (PAR, 400–700 nm).

Site ID	Start-EDT	End-EDT	K_d (m^{-1})	Chl *a* ($\mu g\,l^{-1}$)	CDOM (μg QS l^{-1})	TSS ($mg\,l^{-1}$)	FSS ($mg\,l^{-1}$)	Salinity gradient (%)
NR30	08:48	09:03	3.0	39.8±5.25	60.6±1.12	8.8±0.53	2.8±0.2	128.2
NR50	09:12	09:26	2.5	42.9±5.87	51.8±2.86	7.5±1.1	1.3±0.5	70.1
NR70	09:41	09:53	2.1	29.3±2.52	41.0±0.4	8.1±1.29	1.4±0.69	13.1
NR120	10:17	10:32	1.8	18.7±0.82	30.0±1.31	13.0±2.08	6.8±1.74	13.3
NR160	11:00	11:16	1.0	11.2±0.92	21.6±0.65	7.4±1.11	2.7±1.22	0.9
NR180	11:49	11:55	0.8	9.0±0.45	19.6±0.1	7.2±1.2	2.3±0.5	2.0
PS1	12:11	12:27	0.7	6.2±0.05	16.8±0.31	5.9±0.64	1.3±0.23	6.8
PS3	08:53	09:17	1.6	13.3±0.2	14.2±0.25	29.5±13.9	21.1±1.64	0.3
PS5	09:52	10:10	2.2	12.1±0.41	14.5±0.42	28.3±0.7	19.6±0.92	0.0
NOAA3	10:40	10:57	1.5	11.1±0.3	15.8±0.17	16.1±0.98	9.9±1.27	4.9
NOAA4	11:53	12:09	1.3	7.3±0.37	11.4±0.72	14.6±3.49	9.1±2.65	0.1
AV1	13:00	13:17	1.4	9.2±0.8	14.4±0.38	13.9±0.83	8.0±1.22	5.9
NOAA5	14:01	14:22	1.4	4.9±0.67	12.0±0.72	12.0±0.4	7.1±0.23	2.7

phytoplankton species present at each field site as measured by the CHEMTAX analysis. The CHEMTAX data indicated that the NRE plankton community was dominated by dinoflagellates during the time of the AVIRIS overflight.

Table 4 shows the results of the comparison between the SeaWiFS OC4 and Case 2 Chl *a* algorithms, the AVIRIS-optimized, and MERIS- and MODIS-simulated ratios. The large discrepancy in performance (R^2=0.39) can be attributed to the fact that the OC4 was negatively impacted by the high levels of CDOM and TSS that interfered with the measurement of the primary Chl *a* absorption feature (figures 3(*a*)–3(*c*)). The SeaWiFS Case 2 algorithm, which uses the secondary Chl *a* absorption feature, performed better (R^2=0.62). However, its performance was

Table 3. Phytoplankton community classification using HPLC and CHEMTAX regression analysis. Values are the fraction in $\mu g\,l^{-1}$ of total Chl *a* attributed to each phytoplankton class. Sampling sites are reported beginning in the upper Neuse River, then extending down river and into the Neuse River and Pamlico Estuary.

Site ID	Chlorophytes	Cryptophytes	Cyanobacteria	Diatoms	Dinoflagellates	Total Chl *a*
NR 30	1.7	0.4	5.0	1.5	17.4	26.0
NR 50	1.8	0.0	4.2	0.2	31.1	37.2
NR 70	1.6	0.4	2.8	0.5	8.7	14.1
NR 120	1.6	0.3	2.7	0.8	5.5	10.9
NR 160	1.1	0.4	3.5	1.0	0.9	6.7
NR 180	1.1	0.3	3.1	0.7	0.5	5.7
PS 1	0.9	0.1	3.0	0.6	0.0	4.5
PS 3	1.0	0.4	2.6	1.9	3.2	9.1
PS 5	0.8	0.4	2.2	2.0	2.1	7.4
NOAA 3	0.8	0.4	2.4	1.9	1.2	6.7
NOAA 4	0.5	0.1	1.1	1.5	1.9	5.2
AV 1	0.6	0.4	2.7	2.3	1.3	7.2
NOAA 5	0.5	0.8	0.9	1.0	1.2	4.4

Table 4. Optimized AVIRIS, MERIS and MODIS simulated results using atmospherically corrected imagery. MERIS and MODIS simulated data were derived from higher resolution than the AVIRIS data. AVIRIS channels that most closely corresponded to those of MERIS and MODIS were used to support simulations. Band (B) identification numbers corresponding to the MODIS and MERIS sensors are indicated.

Sensor/algorithm	Ratio or spectral region	R^2
Chl a		
SeaWiFS OC4	$R^{\max}{}_{(443,\ 490\ \text{or}\ 510)}/R_{558}$	0.39*
SeaWiFS Case II	R_{670}/R_{555}	0.62*
AVIRIS-optimized ratio	R_{674}/R_{693}	0.98*
MODIS-simulated R(B3)/R(B4)	R_{469}/R_{555}	0.85
MERIS-simulated R(B7)/R(B10)	R_{665}/R_{709}	0.80
MERIS-simulated R(B8)/R(B10)	R_{681}/R_{709}	0.86
CDOM		
MODIS-simulated R(B3)/R(B4)	R_{469}/R_{555}	0.90
MERIS-simulated R(B3)/R(B5)	R_{490}/R_{560}	0.80
TSS		
MODIS-simulated R(B1)	$R_{620-670}$	0.55
MERIS-simulated R(B6–13)	$R_{615-875}$	0.59
FSS		
MODIS-simulated R(B1)	$R_{620-670}$	0.64
MERIS-simulated R(B6)	$R_{615-875}$	0.64

* Statistically significant difference (α=0.05).

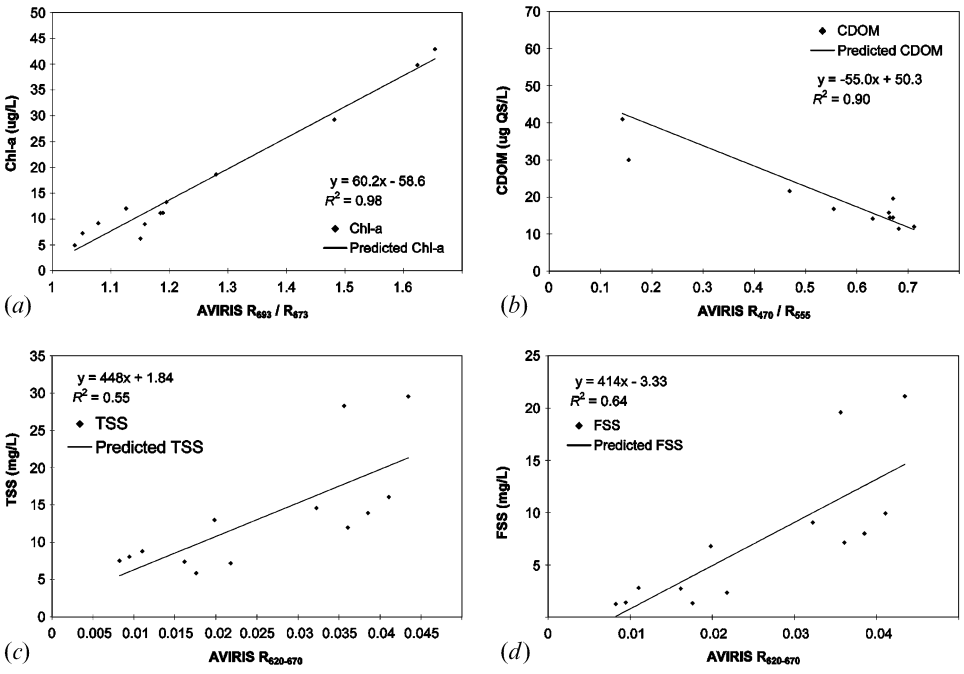

Figure 3. Regression line fit plot of (*a*) AVIRIS Chl *a* ratio, (*b*) CDOM ratio, (*c*) TSS reflectance and (*d*) FSS reflectance to field measurement values. The TSS and FSS plots incorporated multiple AVIRIS bands to simulate a broad-band configuration (620–670 nm).

probably degraded by the high levels of TSS. These results illustrate the importance of using an appropriate model based on the site-specific conditions that correspond to the area of interest.

Figure 3(*a*) illustrates the linear regression fit for the AVIRIS data band ratio *vs.* the field-measured Chl *a* concentrations. The linear regression model was created to quantify the percentage of measured Chl *a* concentrations predicted by the reflectance ratio. The AVIRIS data model had a very high coefficient of determination (R^2=0.98) and was highly significant (α=0.05, $p=2\times10^{-8}$). To evaluate the importance of the atmospheric correction of the AVIRIS data, the Chl *a* regression analysis was repeated for the uncorrected AVIRIS images resulting in an R^2=0.68. This outcome served to indicate the importance of the atmospheric correction. An analysis was also performed to determine the relative performance across the entire VIS and NIR spectral regions to provide a stable baseline to support the secondary Chl *a* absorption feature ratio for the wide range of Chl *a*, CDOM and TSS concentrations encountered. The results presented in figure 4 indicate that the ratio performance using any band located between 693 and 712 nm provided a statistically better result compared to other spectral regions. The results of all three AVIRIS bands within the spectral range provided statistically similar results.

MERIS-simulated data results were used to assess the potential performance for analyses corresponding to both the secondary Chl *a* absorption feature and associated longer wavelength fluorescence features. The results indicated good performance for both ratios with a coefficient of determination of R^2=0.80 corresponding to Chl *a* absorption and R^2=0.86 for fluorescence (table 4). Similarly, MODIS-simulated data results corresponding to the primary Chl *a* absorption

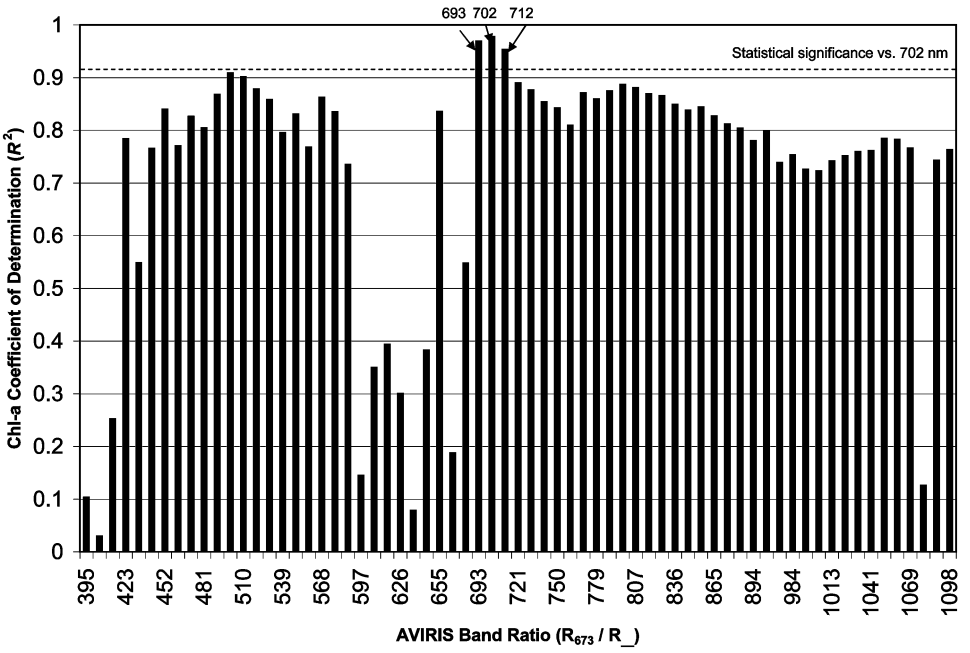

Figure 4. Comparison of regression values for AVIRIS band ratios with 673 nm indicated that the best results were obtained using bands 693, 702 and 712. Additionally, the results obtained for the three bands were not statistically different.

feature for the moderate-resolution model described by Hu *et al.* (2004) also proved to be a good predictor (R^2=0.85).

8.2 *CDOM, TSS and FSS*

The results of the CDOM analysis indicated that the ratio using the AVIRIS-simulated ALI bands 2 and 3 (i.e. 565 and 645 nm) proved to be very good for estimating CDOM concentrations (R^2=0.89) in the NRE (figure 3(*b*)). Similarly, both the MERIS-simulated bands 3 and 5 ratio (i.e. 490 and 560 nm) and MODIS-simulated bands 3 and 4 ratio performed fairly well (R^2=0.80 and R^2=0.90, respectively) (table 4). These results compare well with those reported by Kutser *et al.* (2005) for the correlation between the CDOM absorption coefficient (a_{CDOM} at 420 nm) calculated from *in situ* measurement data and CDOM absorption estimated from atmospherically corrected ALI data for 34 lakes across southern Sweden and Finland and the results of Hu *et al.* (2004) in the Tampa Bay Estuary.

Figure 3(*c*) shows the best result for estimating TSS was a direct linear relationship with MODIS band-1 reflectance (620–670 nm). This relatively poor result (R^2=0.55) did not compare well with that reported by Miller and McKee (2004) for the northern Gulf of Mexico coastal waters. The MERIS simulation using the AVIRIS bands centred at 616.2–874.7 nm (B6–13) also performed similarly (R^2=0.59) using a direct linear regression analysis (table 4). However, some improvement was gained by repeating the analysis for the FSS (table 4). Both the MERIS- and MODIS-simulated reflectance correlations for FSS provided marginally acceptable results (R^2=0.64). The apparent difference in performance between the results reported here and those reported by Miller and McKee (2004) for the Gulf of Mexico can probably be attributed to the fact that Gulf or Mexico TSS was primarily inorganic suspended matter (clay and silt) compared with the inorganic/organic mixture in the NRE. The high concentrations of volatile suspended solids (VSS) apparently limited the potential for predicting suspended solid concentrations.

8.3 *Spatial patterns and distributions*

Figures 5(*a*)–5(*d*) illustrate the estimated Chl *a*, CDOM, TSS and FSS concentrations for the lower Neuse River and upper NRE corresponding to the full-resolution AVIRIS data and best-performing regression models (table 4). The approximately 17 m spatial resolution of the AVIRIS sensor reveals the fine-scale features in Chl *a* concentrations throughout the study area (figure 5(*a*)). These concentration gradients are particularly evident in the upper portion of the image where the Neuse River flows into the estuary. The swirling patterns represent characteristic phytoplankton distributions influenced by both vertical migration and wind-generated wave patterns. (The nearly horizontal linear feature in the upper third of the image is a large bridge spanning the river.) This high-resolution Chl *a* map provides a unique snapshot of phytoplankton distribution on a scale that is not possible using maps created from lower spatial resolution (300 m) satellite data (figures 5(*e*)–5(*h*)). FSS concentration distributions (figures 5(*d*) and 5(*h*)) closely resembled those illustrated for TSS (figures 5(*c*) and 5(*f*)).

The nature and distribution of CDOM was very different from that associated with Chl *a* (figure 5(*b*)). CDOM concentrations tended to be fairly uniform and exhibited diffusion gradients characteristic of a dissolved colorant. The highest concentrations were located in the Neuse River and the northern portion of the NRE

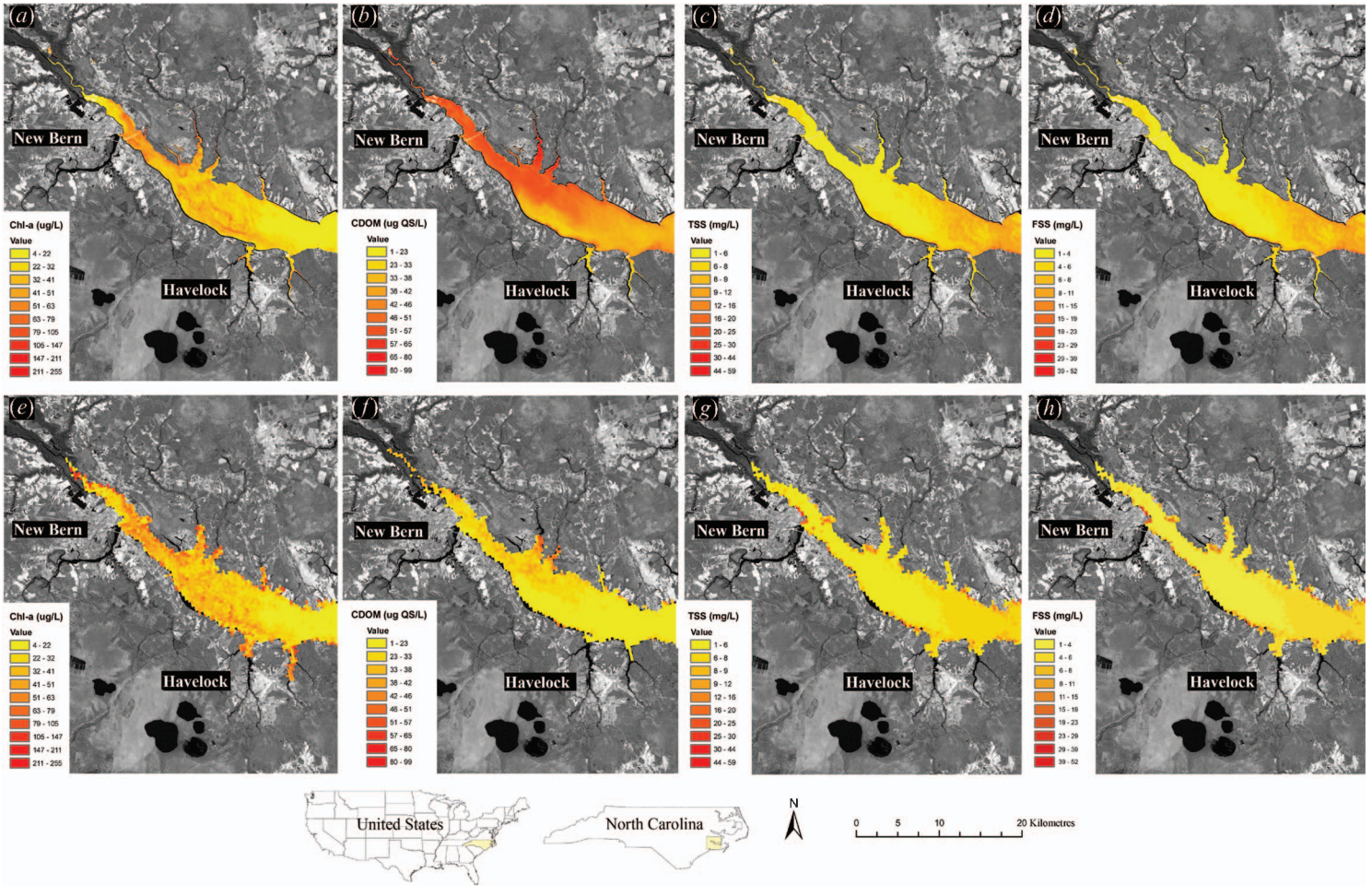

Figure 5. The 17 m resolution AVIRIS predicted concentration distributions for (*a*) Chl *a*, (*b*) CDOM, (*c*) TSS, (*d*) FSS and (*e–h*) coarser resolution (300 m) simulated MERIS distributions across the Neuse River Estuary on 15 May 2002.

and lowest along the southern shoreline (highly developed). The likely sources of CDOM to the system were the upstream riverine wetland communities associated with the Neuse River and the forested wetland complexes located directly adjacent and to the north of the NRE. Illustrated in figure 5(*c*) is the distribution of the TSS concentrations. The TSS organic constituent was resuspended by northwesterly winds associated with a frontal system that passed through the region on 14 May 2002. The suspended material appeared to have largely dissipated from the surface waters in the upper NRE. One possible explanation is that the TSS was associated with the denser water that was transported into the NRE from the Pamlico Sound and established a strong vertical salinity gradient that was documented at sampling sites NR50 (70%) and NR30 (128%) of the NRE (table 2). The FSS concentrations were highly correlated with the TSS (R^2=0.99).

9. Discussion

The results of this work indicate that narrow-band imagery with a high signal-to-noise sensor can be used to estimate surface concentration distributions of Chl *a*, CDOM and FSS in the APES under good atmospheric and water (medium chop) conditions. An important first step before conducting these analyses was atmospheric correction of the imagery data. Conversion of hyperspectral remote sensing data from at-sensor radiance values to surface reflectance has long been recommended for both marine and terrestrial studies. The disparity in Chl *a* correlation coefficients between the pre- and post-corrected AVIRIS data clearly illustrated the importance of atmospheric correction to support water colour estimates for estuarine waters.

The atmospherically corrected AVIRIS images were used to map Chl *a* concentrations with a very high correlation to field-measured values using linear regression analysis. The Chl *a* absorption feature at 673.6 nm, when combined with a longer waveband (690–715 nm) stable portion of the spectrum, resulted in the most robust ratio for Chl *a* estimates. The longer wavelength tended to alleviate much of the TSS interference inherent with shorter wavelength band-derived baselines. The coefficient of determination (R^2=0.98) described an exceptionally strong relationship between the AVIRIS band ratio and the field-measured Chl *a* concentrations. The simulated MERIS and MODIS results corresponding to the Chl *a* fluorescence ratio (R^2=0.86 and 0.85) indicated that an operational satellite monitoring capability is probably feasible. Similarly, the CDOM results optimized for the AVIRIS- and MERIS- and MODIS-simulated data were encouraging (R^2=0.89, 0.80 and 0.90, respectively).

Because of the high cost and low availability of airborne hyperspectral data, the operational use of imaging systems such as AVIRIS data for monitoring water colour is limited. However, occasional under-flights in association with satellite data collections could provide a robust approach for linking field measurements to satellite data to support both empirical model development and validation efforts. The coarser spatial resolution of satellite-based water colour estimates makes direct comparisons with *in situ* sampling data difficult in systems exhibiting complex concentration gradients. The finer-scale airborne data can be scaled to correspond to coarser-scale satellite data to provide a more robust validation approach by bridging the data resolution gap between *in situ* measurement data and medium-resolution satellite data.

In this study, we used the 17 m spatial resolution AVIRIS imagery to simulate 300 m × 300 m MERIS and 500 m × 500 m MODIS imagery by selecting AVIRIS bands centred at or near the MERIS and MODIS bands of interest. Regression

models were developed using the 17 m × 17 m AVIRIS pixels with coincident field measurement data to gain an appreciation of potential performance of MERIS and MODIS data for the APES. Then the 17 m × 17 m pixels were aggregated (simple average) up to 300 m × 300 m MERIS pixel to further assess the utility of the medium-resolution data for APES applications. The regression analysis results indicated that MERIS and MODIS data could be used to adequately estimate Chl *a*, CDOM and FSS concentrations and the aggregated data illustrated that the coarser-resolution data should be useful to monitor the concentrations and general distributions (figures 5(*e*)–5(*h*)). However, the loss of fine system detail apparent with coarser-resolution MERIS-simulated data could make it more difficult to interpret Chl *a* structural dynamics, and identify CDOM sources and diffusion gradients. The 2.8 × coarser resolution of the MODIS (*vs.* MERIS) further limits the potential utility of these data for estuarine applications.

The regression results obtained for TSS were relatively poor (R^2=0.55–0.59), yet highly significant (p=0.03). Problems related to the TSS estimates are thought to be a result of the high levels of VSS in Neuse River and Pamlico Estuaries on 15 May 2002. In a system with very high Chl *a* and CDOM concentrations, the quantification of VSS appears to be a potentially difficult problem. The high concentration of suspended organic matter also probably contributed to the less than optimal FSS results (R^2=0.64).

10. Conclusions

This study demonstrated the potential application of airborne AVIRIS and simulated MERIS and MODIS satellite remote sensor data to quantify Chl *a*, CDOM, TSS and FSS water colour constituents for the APES when simultaneous *in situ* data are available. The results indicated that Chl *a*, CDOM and FSS are potential candidates for operational monitoring using MERIS data. MODIS data could provide similar coefficients of determination; however, the coarser (500 m) spatial resolution associated with the sensor may limit its utility for operational monitoring in the APES. These findings suggest that the MERIS and MODIS (Terra) sensors could potentially be used in combination to provide higher repeat frequency data collections and provide additional spectral data (e.g. 900 nm MERIS and 1240 nm MODIS) to support atmospheric correction of same-day satellite acquisitions. The results also indicate that the optimal sensor band configuration for monitoring estuarine Chl *a* would include the addition of multiple narrow-band passes centred between 665 and 685 nm to provide for optimal band selection for the characterization of secondary Chl *a* absorption and fluorescence peaks. Additional research will be necessary to further quantify the predictive power of these relationships over time across the APES. In addition, the development of a long-term data set would support further study to determine the potential for regression coefficient transference to other geographic locations across the mid-Atlantic region.

The linking of currently available *in situ* water quality monitoring networks, such as the ferry-based monitoring (FerryMon) of surface water quality in the APES (Buzzelli *et al.* 2003), in combination with high-spectral resolution MERIS and medium-spectral resolution MODIS data, could provide a multisensor web capability for the operational monitoring of APES water quality. In particular, MERIS satellite-derived Chl *a* concentration estimates on a 2–3-day cycle for the APES should provide a sufficient monitoring capability to determine the extent and

duration of Chl *a* values that exceed established State of North Carolina TMDL criteria standards. In addition, satellite-derived distributions of Chl *a* and CDOM and TSS concentrations coupled with near-real time FerryMon phytoplankton taxonomic composition could provide useful data to support the development of an operational HAB potential advisory capability. Additional research is needed to determine the viability of an operational capability for estimating TSS concentrations. Separating TSS into inorganic and organic components provided some improvement for estimating the inorganic component (FSS).

Acknowledgements

The U.S. Environmental Protection Agency (EPA) partially funded and partially conducted the research described in this paper. Although this work was reviewed by the EPA and has been approved for publication, it may not necessarily reflect official Agency policy. Mention of any trade names or commercial products does not constitute endorsement or recommendation for use. This research was partially conducted under EPA Cooperative Agreement no. 82867701 and was partially supported by NASA's Earth Sciences Enterprise, Applications Division.

References

ARAR, E.J. and COLLINS, G.B., 1997, *Methods for the Determination of Chemical Substances in Marine and Environmental Matrices*. EPA/600/R-97/072 (Cincinnati, OH: National Exposure Research Laboratory, U.S. Environmental Protection Agency).

BERK, A., BERNSTEIN, L.S. and ROBERTSON, D.C., 1989, *MODTRAN: A Moderate Resolution Model for LOWTRAN 7*. Final report, GL-TR-0122 (Bedford, MA: AFGL, Hanscom AFB).

BRUEGGE, C.J., CONEL, J.E., MARGOLIS, J.S. and GREEN, R.O., 1990, In-situ atmospheric water-vapor retrieval in support of AVIRIS validation. *SPIE Imaging Spectroscopy of the Terrestrial Environment*, **1298**, pp. 150–163.

BUKATA, R.P., JEROME, J.H., KONDRATYEV, K.Y. and POZDNYAKOV, D.V., 1995, *Optical Properties and Remote Sensing of Inland and Coastal Waters* (Boca Raton, FL: CRC Press).

BUZZELLI, C.P., RAMUS, J.R. and PAERL, H.W., 2003, Ferry-based monitoring of surface water quality in North Carolina estuaries. *Estuaries*, **26**, pp. 975–984.

CARDER, K.L., CHEN, F.R., LEE, Z., HAWES, S.K. and CANNIZZARO, J.P., 2003, *MODIS Ocean Science Team Algorithm Theoretical Basis Document: ATBD 19, Case 2 Chlorophyll a* (Version 7). Available online at: http://modis.gsfc.nasa.gov/data/atbd/atbd_mod19.pdf.

COX, C. and MUNK, W., 1954, Statistics of the sea surface derived from sun glitter. *Journal of Marine Research*, **13**, pp. 198–227.

DALL'OLMO, G., GITELSON, A.A., RUNDQUIST, D.C., LEAVITT, B., BARROW, T. and HOLZ, J.C., 2005, Assessing the potential of SeaWiFS and MODIS for estimating chlorophyll concentrations in turbid productive waters using red and near–infrared bands. *Remote Sensing of Environment*, **96**, pp. 176–187.

DEKKER, A.G., HOOGENBOOM, H.J., GODDIJN, L.M. and MALTHUS, T.J.M., 1997, The relation between inherent optical properties and reflectance spectra in turbid inland waters. *Remote Sensing Reviews*, **15**, pp. 59–74.

DRINKWATER, M.R. and REBHAN, H., 2005, *Sentinel-3: Mission Requirements Document*. Final Report: Reference EOP-SMO/1151/MD-md (Noordwijk, The Netherlands: European Space Agency).

GAO, B.C. and GOETZ, F.H., 1990, Column atmospheric water vapor and vegetation liquid retrievals from airborne imaging spectrometer data. *Journal of Geophysical Research*, **95**, pp. 3549–3564.

GILBERT, P.M. and TERLIZZI, D.E., 1999, Cooccurrence of elevated urea levels and dinoflagellate blooms in temperate estuarine aquiculture ponds. *Applied and Environmental Microbiology*, **65**, 5596.

GONS, H.J., RIJKEBOER, M. and RUDDICK, K.G., 2005, Effect of a waveband shift on chlorophyll retrieval from MERIS imagery of inland and coastal waters. *Journal of Plankton Research*, **27**, pp. 125–127.

GORDON, H.R. and WANG, M., 1994, Influence of oceanic whitecaps on atmospheric correction of ocean-color sensors. *Applied Optics*, **33**, pp. 7754–7762.

GREEN, R.O., 1991, Retrieval of reflectance from AVIRIS radiance using a radiative transfer code. In *Proceedings of the Third Airborne Visible/Infrared Imaging Spectrometer (AVIRIS) Workshop*, pp. 200–210, NASA JPL Pub. 91–28 (Pasadena, CA: Jet Propulsion Laboratory).

GREEN, R.O., 1999, Water vapor sensitivity analysis for AVIRIS radiative-transfer-model-based reflectance inversion. In *Proceedings of the Eighth JPL Airborne Earth Science Workshop*, pp. 189–196 (Pasadena, CA: Jet Propulsion Laboratory).

GREEN, R.O., CONEL, J.E. and ROBERTS, D.A., 1993, Estimation of aerosol optical depth and calculation of apparent surface reflectance from radiance measured by the Airborne Visible/Infrared Imaging Spectrometer (AVIRIS) using MODTRAN2. *SPIE Conference*: *Imaging Spectroscopy of the Terrestrial Environment*, Orlando, FL, 14 April, p. 12.

HERUT, B., TIBOR, G., YACOBI, Y.Z. and KRESS, N., 1999, Synoptic measurement of chlorophyll-a and suspended particulate matter from polluted to clean seawater utilizing airborne remote sensing and ground measurements, Haifa Bay (SE Mediterranean). *Marine Pollution Bulletin*, **38**, pp. 762–772.

HOOGENBOOM, H.J., DEKKER, A.G. and ALTHUIS, IJ.A., 1998, Simulation of AVIRIS sensitivity for detecting chlorophyll over coastal and inland waters. *Remote Sensing of Environment*, **65**, pp. 333–340.

HU, C., CHEN, Z., CLAYTON, T.D., SWARZENSKI, P., BROCK, J.C. and MULLER-KARGER, F.E., 2004, Assessment of estuarine water-quality indicators using MODIS medium-resolution bands: initial results from Tampa Bay, FL. *Remote Sensing of Environment*, **93**, pp. 423–441.

JEFFREY, S., MANTOURA, R. and WRIGHT, S. (Eds), 1997, *Phytoplankton Pigments in Oceanography: Guidelines to Modern Methods* (Paris: UNESCO).

KARASKA, M.A., HUGUENIN, R.L., BECHAM, J.L., WANG, M., JENSEN, J.R. and KAUFMANN, R.S., 2004, AVIRIS measurements of chlorophyll, suspended minerals, dissolved organic carbon, and turbidity in the Neuse River, North Carolina. *Photogrammetric Engineering and Remote Sensing*, **70**, pp. 125–133.

KOWALCZUK, P., OLSZEWSKI, J., DARECKI, M. and KACZMAREK, S., 2004, Empirical relationship between coloured dissolved organic matter (CDOM) absorption and apparent optical properties in the Baltic Sea waters. *International Journal of Remote Sensing*, **26**, pp. 345–370.

KRUSE, F.A., 2003, Mineral mapping with AVIRIS and EO-1 Hyperion. In *Proceedings of the 12th JPL Airborne Geoscience Workshop*. 24–28 February 2003, Pasadena, CA. Jet Propulsion Laboratory Publication 04-06 (CD-ROM), pp. 149–156.

KUTSER, T., PIERSON, D.C., KALLIO, K.Y., REINART, A. and SOBEK, S., 2005, Mapping lake CDOM by satellite remote sensing. *Remote Sensing of Environment*, **94**, pp. 535–540.

LAND, P.E. and HAIGH, J.D., 1996, Atmospheric correction over case 2 waters with an iterative fitting algorithm. *Applied Optics*, **35**, pp. 5443–5451.

LI, H.P., GONG, G.C. and HSIUNG, T.M., 2002, Plankton pigment analysis by HPLC and its application in algal community investigations. *Botanical Bulletin of Academia Sinica*, **43**, pp. 283–290.

LIEW, S.C., CHIA, A.S. and KWOH, L.K., 2001, Evaluating the validity of SeaWiFS chlorophyll algorithm for coastal waters. In *Proceedings of the 22nd Asian Conference on Remote Sensing*, Singapore, 5–9 November, p. 5.

LYON, J.G., BEDFORD, K.W., YEN, C.C.J., LEE, D.H. and MARK, D.J., 1988, Determination of suspended sediment concentrations from multiple day Landsat and AVHRR data. *Remote Sensing of Environment*, **25**, pp. 107–115.

MACKEY, M., HIGGINS, H., MACKEY, D. and WRIGHT, S., 1997, *CHEMTAX User's Manual: A Program for Estimating Class Abundances from Chemical Markers – Application to HPLC Measurements of Phytoplankton*. Marine Laboratory Report No. 229 (Hobart, Australia: CSIRO).

MACKEY, M., MACKEY, D., HIGGINS, H. and WRIGHT, S., 1996, CHEMTAX – a program for estimating class abundances from chemical markers: application to HPLC measurements of phytoplankton. *Marine Ecology Progress Series*, **144**, pp. 265–283.

MILLER, L.M. and MCKEE, B.A., 2004, Using MODIS Terra 250 m imagery to map concentrations of total suspended matter in coastal waters. *Remote Sensing of Environment*, **93**, pp. 259–266.

MILLIE, D., PAERL, H. and HURLEY, J., 1993, Microalgal pigment assessments using high-performance liquid chromatography: a synopsis of organismal and ecological applications. *Canadian Journal of Fisheries and Aquatic Science*, **50**, pp. 2513–2527.

NEVILLE, R.A. and GOWER, J.F.R., 1977, Passive remote sensing of plankton *via* chlorophyll-a fluorescence. *Journal of Geophysical Research*, **82**, pp. 3487–3493.

OMERNIK, J.M., 1987, Ecoregions of the conterminous United States. *Annals of the Association of American Geographers*, **77**, pp. 118–125.

O'REILLY, J.E., MARITORENA, S., MITCHELL, B.G., SEIGEL, D.A., CARDER, K.L., GARVER, S.A., KAHRU, M. and MCCLAIN, C., 1998, Ocean color chlorophyll algorithms for SeaWiFS. *Journal of Geophysical Research*, **103**, pp. 24937–24954.

O'REILLY, J.E., MARITORENA, S., SIEGEL, D., O'BRIEN, M.C., TOOLE, D., MITCHELL, B.G., KAHRU, M., CHAVEZ, F.P., STRUTTON, P., COTA, G., HOOKER, S.B., MCCLAIN, C.R., CARDER, K.L., MULLER-KARGER, F., HARDING, L., MAGNUSON, A., PHINNEY, D., MOORE, G.F., AIKEN, J., ARRIGO, K.R., LETELIER, R. and CULVER, M., 2000, Ocean color chlorophyll *a* algorithms for SeaWiFS, OC2, and OC4: version 4. In *SeaWiFS Postlaunch Technical Report Series*. vol. 11 S.B. Hooker and E.R. Firestone (Eds), pp. 9–23. *SeaWiFS Postlaunch Calibration and Validation Analyses, Part 3* (Greenbelt, MD: NASA, Goddard Space Flight Center).

PAERL, H.W., BALES, J.D., AUSLEY, L.W., BUZZELLI, C.P., CROWDER, L.B., EBY, L.A., FEAR, J.M., GO, M., PEIERLS, B.L., RICHARDSON, T.L. and RAMUS, J.S., 2001, Ecosystem impacts of 3 sequential hurricanes (Dennis, Floyd and Irene) on the US's largest lagoonal estuary, Pamlico Sound, NC. *Proceedings of the National Academy of Sciences of the United States of America*, **98**, pp. 5655–5660.

PAERL, H.W., PINCKNEY, J.L., FEAR, J.M. and PEIERLS, B.J., 1998, Ecosystem responses to internal and watershed organic matter loading: consequences for hypoxia in the eutrophying Neuse River Estuary, North Carolina, USA. *Marine Ecology Progress Series*, **166**, pp. 17–25.

PAERL, H.W., VALDES, L.M., PINCKNEY, J.L., PIEHLER, M.F., DYBLE, J. and MOISANDER, P.H., 2003, Phytoplankton pigments as indicators of estuarine and coastal eutrophication. *BioScience*, **53**, pp. 1–12.

PINCKNEY, J.L., PAERL, H.W., HARRINGTON, M.B. and HOWE, K.E., 1998, Annual cycles of phytoplankton community-structure and bloom dynamics in the Neuse River Estuary, North Carolina. *Marine Biology*, **131**, pp. 371–381.

PINCKNEY, J., RICHARDSON, T., MILLIE, D. and PAERL, H., 2001, Application of photopigment biomarkers for quantifying microalgal community composition and in situ growth rates. *Organic Geochemistry*, **32**, pp. 585–595.

PREZELIN, B.B. and ALBERTE, R.S., 1978, Photosynthetic characteristics and organization of chlorophyll in marine dinoflagellates. *Proceedings of the National Academy of Sciences of the United States of America*, **75**, pp. 1801–1804.

ROWAN, K., 1989, *Photosynthetic Pigments of the Algae* (New York: Cambridge University Press).

RUDDICK, K.G., GONS, H.J., RIJKEBOER, M. and TILSTONE, G., 2001, Optical remote sensing of chlorophyll a in case 2 waters by use of an adaptive two-band algorithm with optimal error properties. *Applied Optics*, **40**, pp. 3575–3585.

SCHILLER, H. and DOERFFER, R., 1999, Neural network for emulation of an inverse model: operational derivation of Case II water properties from MERIS data. *International Journal of Remote Sensing*, **20**, pp. 1735–1746.

SHAFIQUE, N.A., AUTREY, B.C., FULK, F. and CORMIER, S.M., 2003, The selection of narrow wavebands for optimizing water quality monitoring in the Great Miami River, Ohio using hyperspectral remote sensor data. *Journal of Spatial Hydrology*, **1**, pp. 1–22.

STAMNES, K. and CONKLIN, P., 1984, A new multi-layer ordinate approach to radiative transfer in vertically in homogeneous atmospheres. *Journal of Quantitative Spectroscopy and Radiative Transfer*, **31**, pp. 273–282.

TESTER, P.A., GEESEY, M.E., GUO, C., PAERL, H.W. and MILLIE, D., 1995, Evaluating phytoplankton dynamics in the Newport River Estuary (North Carolina, USA) by HPLC-derived pigment profiles. *Marine Ecology Progress Series*, **124**, pp. 237–245.

THIEMANN, S. and KAUFMANN, H., 2000, Determination of chlorophyll content and trophic state of lakes using field spectrometer and IRS-1C satellite data in the Mecklenburg Lake district, Germany. *Remote Sensing of Environment*, **73**, pp. 227–235.

VERMOTE, E.F., EL SALEOUS, N.Z. and JUSTICE, C.O., 2002, Atmospheric correction of MODIS data in the visible to middle infrared: first results. *Remote Sensing of Environment*, **83**, pp. 97–111.

WEF, 1998, *Standard Methods for the Examination of Water and Wastewater*. 20th edn (Washington, DC: Water Environment Federation).

WELSCHMEYER, N.A., 1994, Fluorometric analysis of chlorophyll a in the presence of chlorophyll b and pheopigments. *Limnology and Oceanography*, **39**, pp. 1985–1992.

WRIGHT, S., MARCHANT, T.D., HIGGINS, H., MACKEY, M. and MACKEY, D., 1996, Analysis of phytoplankton of the Australian sector of the Southern Ocean: comparisons of microscopy and size frequency data with interpretations of pigment HPLC data using the CHEMTAX matrix factorization program. *Marine Ecological Program Series*, **144**, pp. 285–298.

XIAOXIANG, C., XIAOYING, D. and SI, C., 2004, The study of chlorophyll detection in coastal waters based on environmental variables. In *GIS and Remote Sensing in Hydrology, Water Resources and Environment*, Y. Chen, K. Takara, I. Cluckie and F.H. De Smedt (Eds), No. 289, pp. 316–321 (Wallingford, UK: IAHS Publication).